excellent at most wavelengths. The plateau between 1,700 Å and 3,000 Å is due to a local minimum between two broad absorption features caused by amorphous carbon grains, with the added flat contribution from Fe_3O_4 grains. Silicate grains contribute to the rise at shorter wavelengths.

We conclude that our analysis, combined with observations, provides the first direct evidence for dust produced in supernova ejecta, rather than in evolved stars, in an object at $z > 6$. In particular, we find that dust purely produced by Type-II supernovae can explain the observed extinction curve very well. By implication, we conclude that much of the dust seen at high redshifts probably has the same origin. The properties of high-redshift dust are therefore noticeably different from those found at later cosmic times: grains are typically smaller, owing to their different formation history and to the short time available to subsequently accrete heavy atoms and coagulate with other grains. □

Received 22 April; accepted 6 August 2004; doi:10.1038/nature02930.

1. Hirashita, H. & Ferrara, A. Effects of dust grains on early galaxy evolution. *Mon. Not. R. Astron. Soc.* **337,** 921–937 (2002).
2. Schneider, R., Ferrara, A., Salvaterra, R., Omukai, K. & Bromm, V. Low-mass relics of early star formation. *Nature* **422,** 869–871 (2003).
3. Whittet, D. C. B. *Dust in the Galactic Environment* (Series in Astronomy & Astrophysics, Institute of Physics (IOP) Publishing, Bristol, 2003).
4. Bertoldi, F. *et al.* Dust emission from the most distant quasars. *Astron. Astrophys.* **406,** L55–L58 (2003).
5. Priddey, R. S., Isaak, K. G., McMahon, R. G., Robson, E. I. & Pearson, C. P. Quasars as probes of the submillimetre cosmos at $z > 5$. I. Preliminary SCUBA photometry. *Mon. Not. R. Astron. Soc.* **344,** L74–L78 (2003).
6. Todini, P. & Ferrara, A. Dust formation in primordial Type II supernovae. *Mon. Not. R. Astron. Soc.* **325,** 726–736 (2001).
7. Nozawa, T., Kozasa, T., Umeda, H., Maeda, K. & Nomoto, K. Dust in the early Universe: dust formation in the ejecta of population III supernovae. *Astrophys. J.* **598,** 785–803 (2003).
8. Schneider, R., Ferrara, A. & Salvaterra, R. Dust formation in very massive primordial supernovae. *Mon. Not. R. Astron. Soc.* **351,** 1379–1386 (2004)
9. Moseley, S. H., Dwek, E., Glaccum, W., Graham, J. R. & Lowenstein, R. F. Far-infrared observations of thermal dust emission from supernova 1987A. *Nature* **340,** 697–699 (1989).
10. Dunne, L., Eales, S., Ivison, R., Morgan, H. & Edmunds, M. Type II supernovae as a significant source of interstellar dust. *Nature* **424,** 285–287 (2003).
11. Morgan, H. L., Dunne, L., Eales, S. A., Ivison, R. J. & Edmunds, M. G. Cold dust in Kepler's supernova remnant. *Astrophys. J.* **597,** L33–L36 (2003).
12. Richards, G. T. *et al.* Red and reddened quasars in the Sloan Digital Sky Survey. *Astron. J.* **126,** 1131–1147 (2003).
13. Reichard, T. A. *et al.* Continuum and emission-line properties of broad absorption line quasars. *Astron. J.* **126,** 2594–2607 (2003).
14. Hopkins, P. *et al. Astrophys. J.* (in the press); preprint at ⟨http://arXiv.org/astro-ph/0406293⟩ (2004).
15. Gaskell, C. M., Goosmann, R. W., Antonucci, R. R. J. & Whysong, D. H. The nuclear reddening curve for active galactic nuclei and the shape of the infra-red to X-ray spectral energy distribution. *Astrophys. J.* (submitted); preprint at ⟨http://arXiv.org/astro-ph/0309595⟩ (2003).
16. Maiolino, R. *et al.* Dust in active nuclei. I. Evidence for "anomalous" properties. *Astron. Astrophys.* **365,** 28–36 (2001).
17. Maiolino, R. *et al.* Extreme gas properties in the most distant quasars. *Astron. Astrophys.* **420,** 889–897 (2004).
18. Baffa, C. *et al.* NICS: The TNG Near Infrared Camera Spectrometer. *Astron. Astrophys.* **378,** 722–728 (2001).
19. Maiolino, R., Juarez, Y., Mujica, R., Nagar, N. & Oliva, E. Early star formation traced by the highest-redshift quasars. *Astrophys. J.* **596,** L155–L158 (2003).
20. Hirashita, H., Hunt, L. K. & Ferrara, A. Dust and hydrogen molecules in the extremely metal-poor dwarf galaxy SBS 0335-052. *Mon. Not. R. Astron. Soc.* **330,** L19–L23 (2002).
21. Woosley, S. E. & Weaver, T. A. The evolution and explosion of massive stars. II. Explosive hydrodynamics and nucleosynthesis. *Astrophys. J. Suppl.* **101,** 181–235 (1995).
22. Larson, R. B. Early star formation and the evolution of the stellar initial mass function in galaxies. *Mon. Not. R. Astron. Soc.* **301,** 569–581 (1998).
23. Zubko, V. G., Mennella, V., Colangeli, L. & Bussoletti, E. Optical constants of cosmic carbon analogue grains. I. Simulation of clustering by a modified continuous distribution of ellipsoids. *Mon. Not. R. Astron. Soc.* **282,** 1321–1329 (1996).
24. Scott, A. & Duley, W. W. Ultraviolet and infrared refractive indices of amorphous silicates. *Astrophys. J. Suppl.* **105,** 401–405 (1996).
25. Mukai, T. in *Evolution of Interstellar Dust and Related Topics* (eds Bonetti, A., Greenberg, J. M. & Aiello, S.) 397–446 (Elsevier Science, New York, 1989).

Acknowledgements All authors have contributed equally to this paper. We thank J. Brucato for providing the optical constant of ACAR grains and we thank M. Walmsley for comments. This work was partially supported by the Italian Ministry of Research (MIUR) and by the National Institute for Astrophysics (INAF).

Competing interests statement The authors declare that they have no competing financial interests.

Correspondence and requests for materials should be addressed to R.M. (maiolino@arcetri.astro.it).

Monoenergetic beams of relativistic electrons from intense laser–plasma interactions

S. P. D. Mangles[1], C. D. Murphy[1,2], Z. Najmudin[1], A. G. R. Thomas[1], J. L. Collier[2], A. E. Dangor[1], E. J. Divall[2], P. S. Foster[2], J. G. Gallacher[3], C. J. Hooker[2], D. A. Jaroszynski[3], A. J. Langley[2], W. B. Mori[4], P. A. Norreys[2], F. S. Tsung[4], R. Viskup[3], B. R. Walton[1] & K. Krushelnick[1]

[1]*The Blackett Laboratory, Imperial College London, London SW7 2AZ, UK*
[2]*Central Laser Facility, Rutherford Appleton Laboratory, Chilton, Didcot, Oxon, OX11 0QX, UK*
[3]*Department of Physics, University of Strathclyde, Glasgow G4 0NG, UK*
[4]*Department of Physics and Astronomy, UCLA, Los Angeles, California 90095, USA*

High-power lasers that fit into a university-scale laboratory[1] can now reach focused intensities of more than 10^{19} W cm^{-2} at high repetition rates. Such lasers are capable of producing beams of energetic electrons[2–11], protons[12] and γ-rays[13]. Relativistic electrons are generated through the breaking[9,10,14] of large-amplitude relativistic plasma waves created in the wake of the laser pulse as it propagates through a plasma, or through a direct interaction between the laser field and the electrons in the plasma[15]. However, the electron beams produced from previous laser–plasma experiments have a large energy spread[6,7,9,14], limiting their use for potential applications. Here we report high-resolution energy measurements of the electron beams produced from intense laser–plasma interactions, showing that—under particular plasma conditions—it is possible to generate beams of relativistic electrons with low divergence and a small energy spread (less than three per cent). The monoenergetic features were observed in the electron energy spectrum for plasma densities just above a threshold required for breaking of the plasma wave. These features were observed consistently in the electron spectrum, although the energy of the beam was observed to vary from shot to shot. If the issue of energy reproducibility can be addressed, it should be possible to generate ultrashort monoenergetic electron bunches of tunable energy, holding great promise for the future development of 'table-top' particle accelerators.

Recently, electrons with energies greater than 200 MeV have been observed using ultrashort pulse lasers (the forced laser wakefield regime)[14], while electrons having an energy up to 350 MeV have been observed from laser plasma interactions using petawatt (10^{15} W)-scale lasers[16]. These energies were obtained from acceleration distances of a millimetre or less. However, the electron beams produced from laser–plasma experiments have always previously been observed to have a large energy spread (that is, $\Delta E/E = 100\%$). Although schemes have been proposed to produce monoenergetic beams by injecting electrons into a particular phase of a plasma wave using complex multiple laser beam geometries[17,18] or external electron beams[19], no success has yet been reported. If reproducible monoenergetic beams could be developed, then table-top narrowband femtosecond X-ray sources and free-electron lasers could become a reality, which could potentially lead to significant advances in both medicine and material science. It may also be possible to use the electron bunches generated in this way for injection into conventional radio frequency (RF) accelerators or into subsequent plasma acceleration stages.

The experiment used the Astra laser at the Rutherford Appleton Laboratory to focus ultrashort ($\tau = 40$ fs, 0.5 J) pulses onto a supersonic helium gas-jet (see Fig. 1). The plasma density was varied from $n_e = 3 \times 10^{18}$ cm^{-3} to $n_e = 5 \times 10^{19}$ cm^{-3} by varying the gas-jet pressure. In this density range, the wavelength

of relativistic plasma waves produced ($\lambda_p = 2\pi c/\omega_{pe}$) is between 0.33 and 2 times the laser pulse length ($c\tau = 12\,\mu$m), where $\omega_{pe} = (n_e e^2/m\epsilon_0)^{1/2}$ is the plasma frequency. Over this range of densities, plasma waves are driven by the ponderomotive force of the laser, which is proportional to the intensity gradient of the pulse. The ponderomotive force predominantly pushes electrons forwards (there is also a radial push). Because the ions are much heavier than the electrons and so do not respond to the ponderomotive force, the electrons are dragged back towards their original position by the space charge field. As they overshoot, a plasma oscillation is formed. As the laser beam moves forward through the plasma this sets up a plasma wave travelling in its wake which has a phase velocity equal to the group velocity of the laser pulse in the plasma[20–22]. For low laser intensities, this process is most efficient for pulse lengths where the pulse is shorter than the plasma wavelength. At higher intensities, nonlinear modification of the laser pulse by the plasma wave can efficiently drive plasma waves[14,23], even when this condition is not initially met.

Once established, the plasma wave can then grow until wave-breaking occurs[9,24]. This is where, at very large plasma wave amplitude, the wave motion becomes so nonlinear that wave energy is transferred directly into particle energy. Wave-breaking is not always catastrophic and a proportion of the electrons in the wave can break from the wave, reducing its amplitude, while maintaining the wave structure. Thus this population of injected electrons can continue to interact with the wave and gain further energy.

In our experiment, the electron energy spectrum was measured using an on-axis magnetic spectrometer. A high-resolution image-plate detector (Fuji BAS1800II) was used to obtain the electron spectrum. The electrons were also simultaneously measured using a lower-resolution array of diodes situated behind the image plate in order to calibrate the image plate response. This set-up was able to measure the spectrum over a wide energy range in a single shot.

Electron acceleration was observed over a range of electron densities. With the plasma density below $7 \times 10^{18}\,\mathrm{cm}^{-3}$, no energetic electrons were observed (this corresponds to $\lambda_p = c\tau$). Increasing the density produced a sudden change, with the detection of energetic electrons up to 100 MeV. Measurements of the beam divergence using radiochromic film detectors show that the full-width at half-maximum (FWHM) of the electron beam was less than 5°. However, the most interesting aspect of these spectra is that, in this regime, the electron energy spectra were exceptionally non-maxwellian. Indeed they generally consisted of one or more narrow spiky features, each having an energy bandwidth of less than 20% (see Fig. 2). As the density was increased further, the peak energy of the electrons was observed to decrease and the spectra began to assume a broad maxwellian shape, as reported in previous experiments (see Fig. 2).

The difference observed in these spectra can be attributed to the timing of the injection of electrons into the relativistic plasma wave. Evidently wave-breaking places the electrons to be accelerated at a precise phase within the plasma wave. In this way, all the electrons experience an almost identical acceleration gradient. As the wake-field is several plasma wavelengths in duration, with its amplitude decreasing away from the laser pulse, successive plasma periods can accelerate trapped electron bunches to different energies, producing the multiple spikes in the spectrum.

With careful control of the plasma density and at a higher laser power, the monoenergetic structure was even clearer (Fig. 3); typically, only one very narrow single peak in the spectrum was observed. In this case it is likely that only the first plasma oscillation is driven to breaking point. Note that the total number of electrons in the peak in Fig. 3 is estimated to be about 1.4×10^8 or ~22 pC, with a FWHM energy spread of <3%. Under the same experimental conditions the spectrum consistently showed narrow energy spread, but with variation in the energy of the peak. For shots with the lowest energy spread (<10%) the beam energy varied between 50 and 80 MeV. This is almost certainly due to shot-to-shot variations in the laser parameters.

For these monoenergetic beams to propagate out of the plasma, the electron bunches cannot be dephased (that is, outrun the plasma wave), as then they would be decelerated by the front of the plasma wave. This means that the sum of the length after which wave-breaking occurs and the dephasing length needs to be greater than the interaction length. Indeed, the plasma density regime in which these narrow-energy-spread beams were observed is that where the dephasing length was longer than the observed inter-

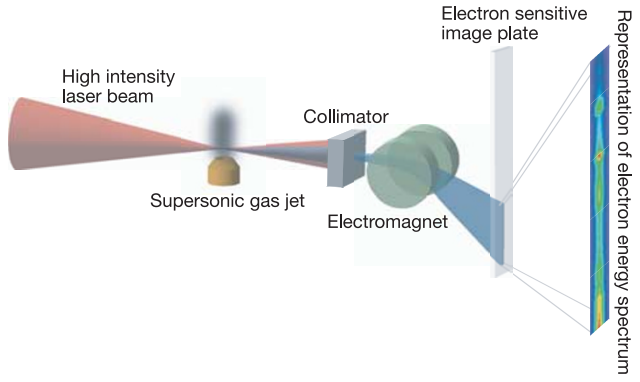

Figure 1 Experimental set-up. The experiment used the high-power titanium:sapphire laser system at the Rutherford Appleton Laboratory (Astra). The laser pulses ($\lambda = 800$ nm, $\tau = 40$ fs with energy approximately 0.5 J on target) were focused with an *f*/16.7 off-axis parabolic mirror onto the edge of a 2-mm-long supersonic jet of helium gas to produce peak intensities up to $2.5 \times 10^{18}\,\mathrm{W\,cm}^{-2}$. The Astra laser has typical shot-to-shot reproducibility for high-power lasers, with variations in pulse energy ±5%, pulse length ±12% and focal spot size ±11%, while the focal spot can move by up to a spot diameter (~25 μm in this case). The electron density (n_e) as a function of backing pressure on the gas jet was determined by measuring the frequency shift ($\Delta\omega = \omega_{pe}$, where ω_{pe} is the electron plasma frequency) of satellites generated by forward Raman scattering in the transmitted laser spectrum[5]. The plasma density was observed to vary linearly with backing pressure within the range $n_e = 3 \times 10^{18}\,\mathrm{cm}^{-3} - 5 \times 10^{19}\,\mathrm{cm}^{-3}$. Electron spectra are measured using an on-axis magnetic spectrometer. Other diagnostics used included transverse imaging of the interaction, and radiochromic film stacks to measure the divergence and total number of accelerated electrons.

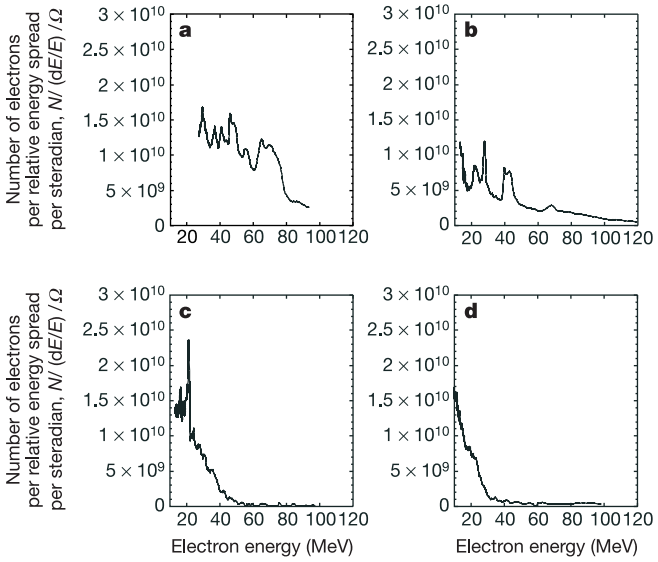

Figure 2 Measured electron spectra at various densities. Laser parameters: $E \approx 350$ mJ, $\tau \approx 40$ fs, $I \approx 1.5 \times 10^{18}\,\mathrm{W\,cm}^{-2}$. Densities ($n_e$, in units of $10^{19}\,\mathrm{cm}^{-3}$): **a**, 1.6; **b**, 1.8; **c**, 3; and **d**, 5.

action length (see Fig. 4). In contrast, at higher densities the dephasing distance is shorter than the interaction distance, and so a quasi-maxwellian distribution of electrons emerges from the plasma (Fig. 2d).

This acceleration mechanism described is supported by particle-in-cell simulations of the interaction, performed using the code OSIRIS[25] on an eight G5 node "Applecluster" at Imperial College London. The simulations were performed over the range of our experimental parameters, and in 2D3V (two spatial but three momentum and field dimensions.) As previously noted[14], 2D3V simulations can underestimate the maximum electron energies, owing to reductions in the degrees of freedom for self-focusing and plasma wave growth. However, they do accurately describe the phenomenology of the interaction.

As in the experiments, the simulations show that for plasma densities for which the plasma wavelength is greater than the pulse length ($\lambda_p \geq c\tau$), a plasma wave is generated, but there is no wave-breaking. At these low densities the forced laser wakefield mechanism[14] is ineffective. But at densities slightly above this threshold, a noticeable change occurs in the interaction. The generation of the plasma wave causes self-focusing of the laser pulse away from its leading edge, owing to the radial density profile of the plasma wave. It is noted that for short pulses relativistic self-focusing is ineffective for the front of the pulse[26]. The laser pulse becomes shaped like a cone, tapered towards the rear, with a length close to λ_p. This causes a feedback mechanism, where the increasing laser intensity towards the back causes the plasma wave amplitude to grow, which can further focus the laser pulse. As the plasma wave reaches large amplitude the longitudinal motion of the electrons in the wave becomes relativistic, which leads to a lengthening of the plasma wavelength.

Crucially, as the laser pulse length is now less than the plasma wavelength, plasma electrons can stream into the plasma wave transversely behind the laser pulse, where previously they were excluded by the laser's ponderomotive force. Because the waveform is non-sinusoidal, a large number of electrons can be injected into a particular phase of the plasma wave and experience an accelerating force. This transverse breaking of the wave reduces the electric field strength of the plasma wave, thus preventing further injection and so ensuring an electron bunch localized in position and time. The transverse injection of electrons can explain why the plasma wave can break at amplitudes significantly less ($E \approx E_0$) than the one-dimensional cold wave-breaking limit, $E_{wb} = \sqrt{2}(\gamma_p - 1)^{1/2}E_0$, where γ_p is the Lorentz factor associated with the plasma wave ($\gamma_p \approx \omega_0/\omega_{pe}$) (ref. 24).

All of the electrons in this bunch then experience very similar acceleration as is demonstrated in Fig. 5, until they begin to outrun the steepened accelerating front of the plasma wave. If the length of

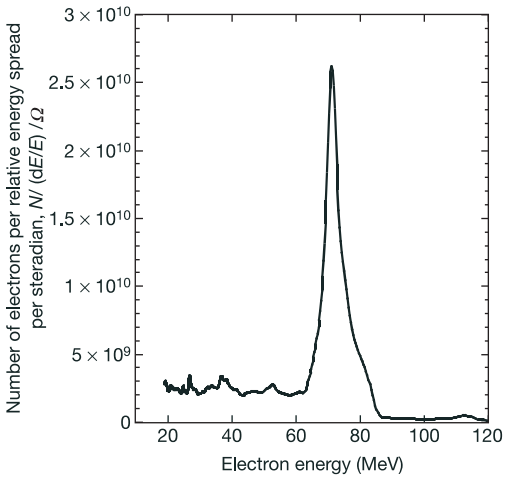

Figure 3 Measured electron spectrum at a density of 2×10^{19} cm^{-3}. Laser parameters: $E = 500$ mJ, $\tau = 40$ fs, $I \approx 2.5 \times 10^{18}$ W cm^{-2}. The energy spread is ±3%. The energy of this monoenergetic beam fluctuated by ~30%, owing to variations in the laser parameters.

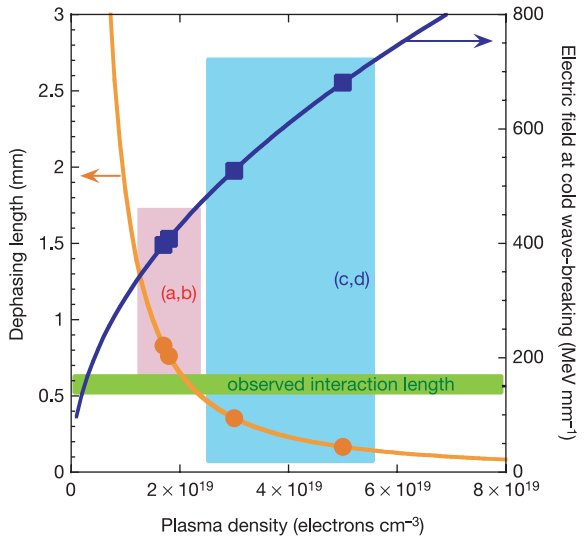

Figure 4 Plot of dephasing length and cold wave-breaking amplitude versus plasma density. Simulations show that the dephasing length in a nonlinear plasma wave remains close to the linear value, $L_d \approx 2\pi c\omega^2/\omega_{pe}^3$, owing to competition between the nonlinearly increasing plasma wavelength, and the decrease in laser pulse group velocity due to photon deceleration. The dephasing lengths (circles) and wave-breaking amplitudes (squares) corresponding to the spectra shown in Fig. 2 are indicated; those in the red shaded region correspond to the spectra that exhibited monoenergetic features, and those in the blue shaded region correspond to the spectra that exhibited maxwellian energy distributions. The green line indicates the interaction length observed using transverse imaging diagnostics.

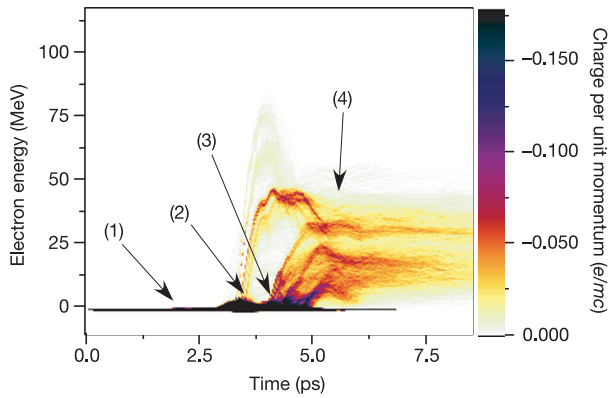

Figure 5 Evolution of the energy spectrum of the electrons (integrated over the two-dimensional simulation box) during a 1 mm interaction at a plasma density of $n_e = 2.1 \times 10^{19}$ cm^{-3}. The simulation space was 1,536 × 1,024 cells (16 cells per λ) with 4 electrons per cell. At the time indicated by the arrow (1) the pulse is self-focused and some relativistic electrons have appeared, but at quite low energies. The laser pulse front begins to steepen owing to the forced wakefield mechanism[14] and this causes the wakefield amplitude to grow. At time (2), the plasma wavelength begins to increase relativistically, and at this point transverse wave-breaking takes place. This bunch experiences a uniform acceleration to high energy. At later time (3), further plasma oscillations, behind the initial one, also break transversely, resulting in multiple bunches of accelerated electrons. As they travel further, these electron bunches begin to dephase with respect to the plasma wave causing energy spread, just before they leave the plasma (4).

the plasma is sufficiently short, then one can extract this monoenergetic bunch, before further wave-breaking of plasma oscillations behind the first causes an increased 'dark-current' of lower-energy electrons (marked (3) in Fig. 5). Indeed, in some simulations this 'dark-current' is found to be greatly reduced if the trailing wake is sufficiently perturbed to prevent efficient trapping and acceleration.

In the simulation shown, the end of the plasma (at $t = 6.6$ ps) is sufficiently close that many of the monoenergetic features remain as they leave the plasma. If the plasma is too long, then the electrons begin to enter a decelerating part of the plasma wave and as a result experience longitudinal energy spread, as can be observed at (4) in Fig. 5. For higher densities, or longer plasmas, this dephasing is complete, and a maxwellian electron energy spectrum results. Such dephasing has been the case in most previous laser-based acceleration experiments, explaining why such features have not been seen before. However, with the right combination of laser pulse length ($c\tau \approx \lambda_p$), focal spot size, plasma density and interaction length, monoenergetic features such as that in Fig. 3 are the principal characteristic of the spectrum of relativistic electrons in both simulations and experiment. □

Received 26 May; accepted 18 August 2004; doi:10.1038/nature02939.

1. Perry, M. D. & Mourou, G. Terawatt to petawatt subpicosecond lasers. *Science* **264,** 917–924 (1994).
2. Key, M. H. *et al.* Hot electron production and heating by hot electrons in fast ignitor research. *Phys. Plasmas* **5,** 1966–1972 (1998).
3. Tajima, T. & Dawson, J. Laser electron accelerator. *Phys. Rev. Lett.* **43,** 267–270 (1979).
4. Joshi, C. & Katsouleas, T. Plasma accelerators at the energy frontier and on tabletops. *Phys. Today* **56,** 47–53 (2003).
5. Esarey, E., Sprangle, P., Krall, J. & Ting, A. Overview of plasma-based accelerator concepts. *IEEE Trans. Plasma Sci.* **24,** 252–288 (1996).
6. Wagner, R., Chen, S. Y., Maksimchuk, A. & Umstadter, D. Electron acceleration by a laser wakefield in a relativistically self-guided channel. *Phys. Rev. Lett.* **78,** 3125–3128 (1997).
7. Ting, A. *et al.* Plasma wakefield generation and electron acceleration in a self-modulated laser wakefield accelerator experiment. *Phys. Plasmas* **4,** 1889–1899 (1997).
8. Tzeng, K. C. & Mori, W. B. Suppression of electron ponderomotive blowout and relativistic self-focusing by the occurrence of Raman scattering and plasma heating. *Phys. Rev. Lett.* **81,** 104–107 (1998).
9. Modena, A. *et al.* Electron acceleration from the breaking of relativistic plasma waves. *Nature* **377,** 606–608 (1995).
10. Santala, M. I. K. *et al.* Observation of a hot high-current electron beam from a self-modulated laser wakefield accelerator. *Phys. Rev. Lett.* **86,** 1227–1230 (2001).
11. Pukhov, A. & Meyer-ter-Vehn, J. Laser wake field acceleration: the highly non-linear broken-wave regime. *Appl. Phys. B* **74,** 355–361 (2002).
12. Clark, E. L. *et al.* Measurements of energetic proton transport through magnetized plasma from intense laser interactions with solids. *Phys. Rev. Lett.* **84,** 670–673 (2000).
13. Edwards, R. D. *et al.* Characterization of a gamma-ray source based on a laser-plasma accelerator with applications to radiography. *Appl. Phys. Lett.* **80,** 2129–2131 (2002).
14. Malka, V. *et al.* Electron acceleration by a wake field forced by an intense ultrashort laser pulse. *Science* **298,** 1596–1600 (2002).
15. Pukhov, A., Sheng, Z. M. & Meyer-ter-Vehn, J. Particle acceleration in relativistic laser channels. *Phys. Plasmas* **6,** 2847–2854 (1999).
16. Mangles, S. P. D. *et al.* Electron acceleration to 350 MeV due to the direct interaction of an ultra-intense laser pulse with an underdense plasma. *Phys. Rev. Lett.* (submitted).
17. Umstadter, D. Review of physics and applications of relativistic plasmas driven by ultra-intense lasers. *Phys. Plasmas* **8,** 1774–1785 (2001).
18. Umstadter, D., Kim, J. K. & Dodd, E. Laser injection of ultrashort electron pulses into wakefield plasma waves. *Phys. Rev. Lett.* **76,** 2073–2076 (1996).
19. Amiranoff, F. *et al.* Observation of laser wakefield acceleration of electrons. *Phys. Rev. Lett.* **81,** 995–998 (1998).
20. Sprangle, P., Esarey, E. & Ting, A. Nonlinear interaction of intense laser pulses in plasmas. *Phys. Rev. A* **41,** 4463–4467 (1990).
21. Bulanov, S. V., Kirsanov, V. I. & Sakharov, A. S. Excitation of ultrarelativistic plasma waves by pulse of electromagnetic radiation. *JETP Lett.* **50,** 198–201 (1989).
22. Berezhiani, V. I. & Murusidze, I. G. Relativistic wake-field generation by an intense laser-pulse in a plasma. *Phys. Lett. A* **148,** 338–340 (1990).
23. Sprangle, P., Esarey, E., Ting, A. & Joyce, G. Laser wakefield acceleration and relativistic optical guiding. *Appl. Phys. Lett.* **53,** 2146–2148 (1988).
24. Akhiezer, A. I. & Polovin, R. V. Theory of wave motion of an electron plasma. *JETP* **3,** 696–705 (1956).
25. Fonseca, R. A. *et al. Lecture Notes in Computer Science* Vol. 2329, III-342 (Springer, Heidelberg, 2002).
26. Faure, J. *et al.* Effects of pulse duration on self-focusing of ultra-short lasers in underdense plasmas. *Phys. Plasmas* **9,** 756–759 (2002).

Acknowledgements This work was supported by the UK EPSRC and RCUK. We thank the OSIRIS consortium (UCLA/IST Lisboa/USC) for the use of OSIRIS, and S. Karsch for discussions.

Competing interests statement The authors declare that they have no competing financial interests.

Correspondence and requests for materials should be addressed to S.M. (stuart.mangles@imperial.ac.uk).

High-quality electron beams from a laser wakefield accelerator using plasma-channel guiding

C. G. R. Geddes[1,2], Cs. Toth[1], J. van Tilborg[1,3], E. Esarey[1], C. B. Schroeder[1], D. Bruhwiler[4], C. Nieter[4], J. Cary[4,5] & W. P. Leemans[1]

[1]*Lawrence Berkeley National Laboratory, 1 Cyclotron Road, Berkeley, California 94720, USA*
[2]*University of California, Berkeley, California 94720, USA*
[3]*Technische Universiteit Eindhoven, Postbus 513, 5600 MB Eindhoven, the Netherlands*
[4]*Tech-X Corporation, 5621 Arapahoe Ave. Suite A, Boulder, Colorado 80303, USA*
[5]*University of Colorado, Boulder, Colorado 80309, USA*

Laser-driven accelerators, in which particles are accelerated by the electric field of a plasma wave (the wakefield) driven by an intense laser, have demonstrated accelerating electric fields of hundreds of GV m^{-1} (refs 1–3). These fields are thousands of times greater than those achievable in conventional radio-frequency accelerators, spurring interest in laser accelerators[4,5] as compact next-generation sources of energetic electrons and radiation. To date, however, acceleration distances have been severely limited by the lack of a controllable method for extending the propagation distance of the focused laser pulse. The ensuing short acceleration distance results in low-energy beams with 100 per cent electron energy spread[1–3], which limits potential applications. Here we demonstrate a laser accelerator that produces electron beams with an energy spread of a few per cent, low emittance and increased energy (more than 10^9 electrons above 80 MeV). Our technique involves the use of a preformed plasma density channel to guide a relativistically intense laser, resulting in a longer propagation distance. The results open the way for compact and tunable high-brightness sources of electrons and radiation.

Previous laser driven plasma acceleration experiments have used a single intense (10^{18}–10^{19} W cm^{-2}) laser pulse propagating in the plasma formed when the front edge of the pulse ionized the gas plume emanating from a jet. The laser power was above the critical power for self-focusing and the laser pulse length exceeded the plasma period[6]. In this so-called self-modulated wakefield regime[6], some self-guiding of the laser pulse occurs owing to relativistic modification of the plasma refractive index, but the laser pulse is highly unstable[7]. Large plasma waves, or wakes, can be driven by the radiation pressure of the intense laser, but the propagation length is limited to little more than the diffraction or Rayleigh length, Z_R (refs 5, 8). The best results have hence been obtained by increasing the laser spot size to increase Z_R, requiring ever greater laser power, but this approach has still been limited to distances of a few hundred micrometres (ref. 8). Plasma electrons were trapped and accelerated in the resulting high-amplitude plasma wave, and electron bunches with 100% energy spread and an exponentially small fraction of electrons at high energy were observed. For example, using a 32 TW